E2V-SDE: From Asynchronous Events to Fast and Continuous Video Reconstruction via Neural Stochastic Differential Equations

Jongwan Kim[1] DongJin Lee[2] Byunggook Na[2]
Seongsik Park[4] Jeonghee Jo[2] Sungroh Yoon[1,2,3*]
[1] Interdisciplinary Program in AI, Seoul National University
[2] Department of ECE, Seoul National University
[3] AIIS, ASRI, INMC, ISRC, Seoul National University
[4] Korea Institute of Science and Technology

Abstract

Event cameras respond to brightness changes in the scene asynchronously and independently for every pixel. Due to the properties, these cameras have distinct features: high dynamic range (HDR), high temporal resolution, and low power consumption. However, the results of event cameras should be processed into an alternative representation for computer vision tasks. Also, they are usually noisy and causes poor performance in areas with few events. In recent years, numerous researchers have attempted to reconstruct videos from events. However, they do not provide good quality videos due to a lack of temporal information from irregular and discontinuous data. To overcome these difficulties, we introduce an E2V-SDE whose dynamics are governed in a latent space by Stochastic differential equations (SDE). Therefore, E2V-SDE can rapidly reconstruct images at arbitrary time steps and make realistic predictions on unseen data. In addition, we successfully adopted a variety of image composition techniques for improving image clarity and temporal consistency. By conducting extensive experiments on simulated and real-scene datasets, we verify that our model outperforms state-of-the-art approaches under various video reconstruction settings. In terms of image quality, the LPIPS score improves by up to 12% and the reconstruction speed is 87% higher than that of ET-Net.

1. Introduction

Event cameras asynchronously measure per-pixel brightness changes in the scene and output a stream of events. Event cameras have attractive characteristics compared to conventional frame cameras: high dynamic range, high temporal resolution, and low power consumption, and high pixel bandwidth resulting in reduced motion blur. Despite the advantages of the event cameras, it is still difficult to apply directly to the computer vision tasks. Because the outputs of event cameras are processed into an alternative representations such as event image [28] or 3D voxel grid [43] to apply to the tasks.

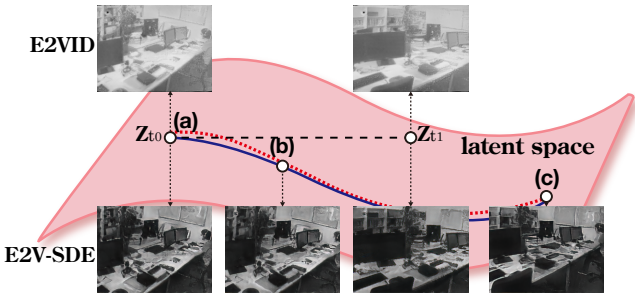

Figure 1. Strength of E2V-SDE compared to E2VID: (a) high-quality image reconstruction, (b) continuous time state, (c) interpolation and extrapolation. The pink surface means latent space. The red dotted line indicates ground truth, blue solid line is E2V-SDE and dashed black line indicates latent state of E2VID.

In [8], the streams of events contain the entire visual signal in a highly compressed form, which can be decompressed to recover a video with arbitrarily high frame rates. However, since the streams are noisy and sparse, reconstructing images through them is an ill-posed problems [4].

Many studies have been proposed to reconstruct frames from events, but the quality of results and reconstruction speed are still unsatisfactory. Recently, deep neural network based reconstruction models [34, 37, 44] have demonstrated impressive performance. However, they are an awkward fit for irregularly-sampled time series data. A standard trick for applying models to irregular time series is to divide the timeline into equally-sized intervals, and impute or aggregate observations using averages. Such preprocessing destroys temporal information, particularly about the timing

*Corresponding Author

of measurements, which can be informative about latent variables [3, 21, 24].

An approach which better matches reality is to construct a continuous-time model with a latent state defined at all times [1]. They generalize state transitions to continuous time dynamics specified by a neural network, as in neural ordinary differential equations (ODE) [3]. However, these methods generally assume the determinant process except randomness, which strongly limits their ability to model complex continuous-time stochastic processes.

Compared to ODE, stochastic differential equation (SDE) is more practical solution for modeling continuous-time stochastic processes [14, 15] and robust against noise [23]. Some studies tried to approximate stochastic processes from the data, most of these methods define system dynamics as linear models, which do not represent high-dimensional data with nonlinear relationships well [25].

In this paper, we propose a new continuous-time stochastic video reconstruction model called E2V-SDE, which effectively reconstructs images from events through SDE. We summarize our contributions as follows:

- To overcome the typical limitations of event-based video reconstruction methods, we propose a new model called E2V-SDE whose latent dynamics is governed by SDEs. Therefore, E2V-SDE can handle irregularly-sampled time series data and reconstruct frames at any arbitrary time steps due to the continuous nature of SDEs.

- We propose an effective model architecture for reliable training and reconstruction and theoretically prove it. To the best of our knowledge, this is the first stochastic video reconstruction model in the literature that combines an adversarial loss with a latent variable model trained via the variational lower bound. In addition, various image composition techniques are used to maintain the sharpness of reconstructed frames.

- To reveal the outstanding performance of E2V-SDE, we conduct extensive experiments. Our model outperforms the state-the-of-art methods in terms of the quality of reconstruction while maintaining a relatively short inference time. We further present the results of the interpolation and extrapolation possible due to the distinct feature of the continuous-time dynamics model.

2. Related Works

2.1. Event-based Video Reconstruction

Early reconstruction works are based on hand-crafted features to estimate intensity from events [5, 16]. Kim *et al*. [16] utilized a Kalman filter to reconstruct brightness gradient maps that can be transferred into intensity images. Cook *et al*. [5] proposed recurrently interconnected maps to reconstruct the intensity images from event cameras. More recent studies on event-based video reconstruction have achieved significant results with the assistance of deep learning. In particular, approaches that employ convolutional neural networks (CNNs) have proven their effectiveness in generating high-quality images from events. In [34], E2VID, a convolutional recurrent neural network based on the UNet [35], was proposed with an explicit temporal consistency loss to reconstruct high-resolution images. Firenet [37] significantly reduced the size of the architecture and image reconstruction speed compared with E2VID. Wang *et al*. [43] was the first to use generative adversarial networks (GANs) in the event vision domain, successfully reconstructing images and high frame rate videos from events. More recently, a transformer [42] structure was applied to event-based video reconstruction [44]. However, these models do not fully utilize temporal information and cannot generate frames at arbitrary times.

2.2. Stochastic Differential Equation

Recently, the neural ODE [3] opened the way for a novel, continuous representation of neural networks by applying a deep learning model to approximate continuous-time dynamics. The hidden state is defined at all times, and can be evaluated at any desired times using a numerical ODE solver. However, these methods generally assume the determinant process except randomness, which strongly limits their ability to model complex continuous-time stochastic processes.

Compared to ODEs, SDEs [18] are more practical solutions for modeling continuous time stochastic processes. More recent works [13, 22] adopted stochastic term in their ODE solvers. This stochasticity injects the model with slight random noise to improve the generalization ability and noise robustness compared to ODE-based methods [23]. SDE solvers [41] were developed through stochastic automatic differentiation based on the Wiener process. Similarly, a few studies [10, 12] incorporated the standard Brownian motion [30], so that the stochastic process should follow a Gaussian distribution with zero mean and variance t. Li *et al*. [20] introduced a stochastic adjoint sensitivity method [7] for simple and practical fitting SDE problems. Other works [18, 29, 32, 38] are proposed for various SDE solver types in neural networks. Models based on SDE have been successfully adopted in numerous applications. This continuous-depth approach showed remarkable performance in various tasks, such as time-series generation [26, 40], density estimation [6, 36], or other supervised learning.

3. Preliminaries

3.1. Stochastic Differential Equations

SDEs can be viewed as a stochastic analogue of ordinary differential equations in the sense that $\frac{\mathrm{d}\boldsymbol{Z}_t}{\mathrm{d}t} = \mu(\boldsymbol{Z}_t, t) + \epsilon \cdot (\boldsymbol{Z}_t, t)$, where $\epsilon \sim \mathcal{N}(0, \mathbf{I})$. Following Kidger *et al.* [15], we construct Neural SDEs with a certain amount of structure. Let $T > 0$ be fixed and $\boldsymbol{Z}_t$ is a variable that continuously evolves over time. An m-dimensional SDE describing the stochastic dynamics of $\mathbf{Z}_t$ usually takes the form as follows:

$$\mathrm{d}\mathbf{Z}_t = \mu_\theta(\mathbf{Z}_t, t)\mathrm{d}t + \sigma_\theta(\mathbf{Z}_t, t)\mathrm{d}W_t, \tag{1}$$

where μ_θ and σ_θ are neural network, $\mu_\theta : [0, T] \times \mathbb{R}^k \to \mathbb{R}^k, \sigma_\theta : [0, T] \times \mathbb{R}^k \to \mathbb{R}^{k\times w}$. Collectively these are parameterized by θ. $W : [0, T] \to \mathbb{R}^m \times k$ is a k-dimensional Wiener process, which is also called standard Brownian motion. The dimension k is a hyperparameter describing the dimension of latent state. The solution of an SDE is a continuous-time stochastic process $\boldsymbol{Z}_t$ that satisfies the integral equation $\boldsymbol{Z}_t = \boldsymbol{Z}_0 + \int_0^t \mu(\boldsymbol{Z}_s, s)\mathrm{d}s + \int_0^t \sigma(\boldsymbol{Z}_s, s)\mathrm{d}W_s$ with an initial condition $\boldsymbol{Z}_0$. The stochastic integral should be interpreted as a traditional Itô integral. For each sample trajectory $w \sim W_t$, the stochastic process $\boldsymbol{Z}_t$ maps w to a different trajectory $\boldsymbol{Z}_t(w)$.

SDEs have been used as models of latent dynamics in a variety of contexts [9, 20]. As closed-form finite-dimensional solutions to SDEs are rare, variational approximations are often used in practice. Li *et al.* [20] proposed a principled way of re-weighting the trajectories of latent SDEs for variational approximations using Girsanov's theorem [31]. They combine adjoint approach with a gradient-based stochastic variational inference scheme for efficiently marginalizing over latent SDE models with arbitrary differentiable likelihoods. Furthermore, let $p(\boldsymbol{x} \mid \boldsymbol{Z}_t)$ denote the probability of observing $\boldsymbol{x}$ conditioned on the trajectory of the latent process $\boldsymbol{Z}_t$ in the interval $[0, T]$. If there exists a mapping $u : \mathbb{R}^m \times [0, T] \to \mathbb{R}^k$ such that $\sigma(\boldsymbol{Z}, t)u(\boldsymbol{Z}, t) = \mu_2(\boldsymbol{Z}, t) - \mu_1(\boldsymbol{Z}, t)$ and u satisfies Novikov's condition [31], the variational lower bound is as follows:

$$\log p(\boldsymbol{x}) = \log \mathbb{E}\left[\log[p(\boldsymbol{x} \mid \widehat{\boldsymbol{Z}}_t)] + \log \boldsymbol{M}_T\right],$$
$$\boldsymbol{M}_T = \exp\Big(-\int_0^T \frac{1}{2}\left|u(\widehat{\mathbf{Z}}_t, t)\right|^2 \mathrm{d}t - \int_0^T u(\widehat{\boldsymbol{Z}}_t, t)^T \mathrm{d}W_t\Big).$$

Detailed proof and full derivation are given in the appendix.

4. Method

4.1. Event Representation

Event e encodes the location, time, and sign of the brightness changes, that is, $e = (x, y, t, p)$, where (x, y) is the triggered coordinates in the image, t is the time of the event, and $p \in \{\pm 1\}$ is the polarity of the brightness change. Then, the event generation process can be expressed as

$$\log(\mathbb{I}_{x,y}) - \log(\mathbb{I}_{x,y}(t - \Delta t)) = p\tau, \tag{2}$$

where τ is the contrast threshold, $\mathbb{I}_{x,y}(t)$ is the intensity at time t and location (x, y), and Δt is a small time period.

The raw event stream $\mathcal{E} = \{\boldsymbol{e}_i\}_{i=0}^{N-1}$, where N represents the total number of events, needs to be fed into the network. As in previous studies [34, 44], we divide the incoming stream of events into sequential, non-overlapping spatio-temporal stream $\mathcal{E}_{t_i}$. $\mathcal{E}_{t_i}$ has the number of fixed events n_e where $i \in [0, T]$, $T \triangleq N/n_e$.

After $\mathcal{E}$ is partitioned, each $\mathcal{E}_{t_i}$ is converted into a grid-type voxel $\boldsymbol{E}_{t_i} \in \mathbb{R}^{B\times H\times W}$ with B time bins via temporal bilinear interpolation, which is expressed as follows:

$$\begin{aligned} \boldsymbol{E}_{(x_l, y_m, t_n)} &= \sum_{x_i = x_l, y_i = y_m} p_i \max(0, 1 - |t_n - t_i^*|), \\ t_i^* &= (B - 1) \times \frac{t_i - t_{min}}{t_{max} - t_{min}}, \end{aligned} \tag{3}$$

where t_{min} and t_{max} denote the timestamps of the first and the last events in $\mathcal{E}$, respectively, and $t_n \in [0, B - 1]$.

4.2. Encoder

As mentioned in preliminaries3.1, we use a variational approximation of the observational log-likelihood for both training and inference. Desirable variational approximations rely on variational posteriors that are close enough to the true posterior of the latent trajectory conditioned on observations. In (1), μ and σ are often referred to as drift and diffusion function, respectively.

The grid type voxel $\boldsymbol{E}_i$ is passed through encoder to input the latent space. We propose the SDE-ConvGRU architecture, a combination of neural SDE and ConvGRU specifically designed to capture not only temporal but also spatial features from the input event streams. Compared to autoregressive model, we separate the dynamic of the state representations from the generated frames. By removing a link between frame synthesis and temporal dynamics, this is computationally appealing when coupled with a low-dimensional latent space. We define the state between observations to be the solution to an SDE.

$$\begin{cases} d\boldsymbol{Z}_t = \mu_\theta(\boldsymbol{Z}_t, t)\mathrm{d}t + \sigma_\theta(\boldsymbol{Z}_t, t)\mathrm{d}W_t, \\ \boldsymbol{Z}_{t+\Delta t} = \boldsymbol{Z}_t + \mu_\theta(\boldsymbol{Z}_t, t)\Delta t + \sigma_\theta(\boldsymbol{Z}_t, t)\sqrt{\Delta t}W_t \\ \boldsymbol{Z}_{t+1} = \mathrm{ConvGRUCell}(\boldsymbol{Z}_t, \boldsymbol{E}_t), \end{cases}$$

where $\boldsymbol{Z}_t \in \mathbb{R}^{m'\times n'\times c'}$ is a latent state of size $m' \times n'$ with c' channels at t_i and f_θ is a ConvGRU. In tandem with the latent state $\boldsymbol{Z}_i$, the ConvGRU derives the updated

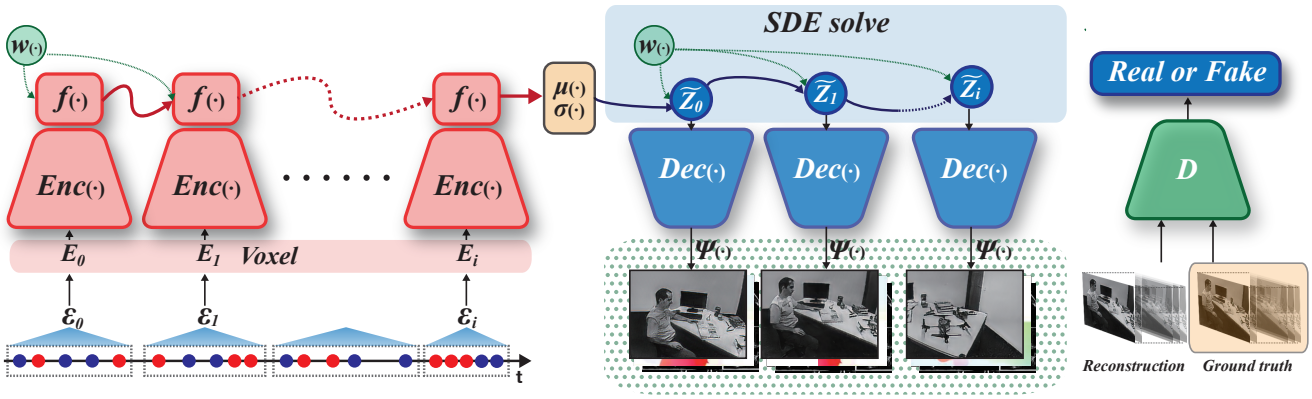

Figure 2. Overview of E2V-SDE. The stream of events (depicted as red/blue dots on the time axis) is partitioned into $\boldsymbol{E}_i$. The events in each window are then converted into a voxel $\boldsymbol{E}_i$ and fed into a encoder to produce latent state $\boldsymbol{Z}_i$, which becomes the input of f_θ. The final latent state $\boldsymbol{Z}_T$ is used as an initial value by another SDE solver which sequentially updates the latent state. Given the initial state $\boldsymbol{Z}_0$ and a Brownian motion sample path $\boldsymbol{w}(\cdot)$, the intermediate states $\boldsymbol{Z}_1, \ldots, \boldsymbol{Z}_i$ are deterministically approximated by a numerical SDE solver. The states are converted intro realistic frames through decoder and linear composition techniques $\Psi(\cdot)$. A discriminator $\boldsymbol{D}$ determines whether the reconstructed frame is real or fake based on ground truth image.

state and then captures the spatio-temporal dynamics of sequences effectively. We assume that both μ and σ have infinitely many bounded derivatives with respect to the state, and bounded first derivatives with respect to time. Therefore, the SDE has a unique strong solution because μ, σ are globally $Lipschitz$ condition in the state. For more detailed demonstration about the uniqueness, see the appendix.

4.3. Decoder

deWe use a latent-variable time-series model, which is defined by SDE, whose initial latent state $\boldsymbol{Z}_T$ is determined in the posterior. The decoder generates a sequence of frames at target timesteps based on the latent representation $\boldsymbol{Z}_{t_i}$ of the input event streams $\boldsymbol{E}_{t_i}$ produced by the encoder. For reconstruction from $\boldsymbol{Z}_{t_i}$. E2V-SDE consists of an SDE solver, decoder g and linear composition Ψ. The dynamics of the latent state can be described as

$$\begin{cases} \mathrm{d}\widetilde{\boldsymbol{Z}}_i = \mu_\phi(\widetilde{\boldsymbol{Z}}_t, t)\mathrm{d}t + \sigma_\phi(\widetilde{\boldsymbol{Z}}_t, t)\mathrm{d}W_t, \\ \mathcal{F}_i, \mathcal{D}_i, \mathcal{M}_i = g_\phi(\widetilde{\boldsymbol{Z}}_{i-1}, \widetilde{\boldsymbol{Z}}_i), \\ \widetilde{\mathcal{I}}_{t_i} = \Psi(\mathcal{M}_{t_i} \odot \mathcal{W}(\mathcal{F}_{t_i}, \widetilde{\mathcal{I}}_{t_{i_1}}) + (1 - \mathcal{M}_{t_i}) \odot \mathcal{D}_{t_i}), \end{cases}$$

where $\mathcal{F}_i$ is a optical flow, $\mathcal{M}_i$ is a composition mask, $\mathcal{W}$ is a warping and $\mathcal{D}_i$ is a image difference. Given the initial value $\widetilde{\boldsymbol{Z}}_0$, the latent generative process is defined by SDEs. The SDEs determine the trajectory followed in latent space from the initial condition with respect the latent vectors predicted along the trajectory at provided times is used to independently sample predicted frame.

Compared to a regular RNN, this simple principle makes our temporal model lighter and more interpretable. Eq. (4.3), however, differs from a discretized ODE because of the introduction of the stochastic wiener variables w.

4.4. Linear Composition

Optical Flow ($\mathcal{F}_{t_i}$) Optical flow is defined as the offset between corresponding pixels in a pair of images $(\mathcal{I}_{t-1}, \mathcal{I}_t)$ between the adjacent images. The collection of the offsets on an image is defined as a flow map $\mathcal{F}_i$. Optical flow uses a first-order approximation method based on a linear relation between adjacent frames. Optical flow successfully handle simple motion, they still have limitations in highly dynamic scenarios. Therefore, directly warping the image using only optical flow generates 'ghosting effect' due to occlusion [46] that some pixels in the first image do not have correspondences in the second image.

Image Difference ($\mathcal{D}_i$) In order to solve the aforementioned problems, we employ the image difference $\mathcal{D}_i \in \mathbb{R}^{m \times n \times c}$ at each i, which predicts the pixel-wise difference between the current frame and the previous frame. Including $\mathcal{D}_i$ helps our model focus on areas where sudden movements take place.

Flow Valid Mask ($\mathcal{M}_i$) The frame $\mathcal{I}_i$ is generated by combining $\mathcal{W}(\cdot)$ and $\mathcal{D}_i$, using element-wise convex combination weighted by the mask $\mathcal{M}_i \in \mathbb{R}^{m \times n}$. While outputs of the g_ϕ have values in $[-\infty, \infty]$, $\mathcal{M}_i$ is forced to values in $[0, 1]$ by passing by a sigmoid activation, in order to perform its role as the convex combination weight. We demonstrate the component in Table 3.

4.5. Objective Functions

4.5.1 Reconstruction Loss

Each frame $\widetilde{\mathcal{I}}_i$ is generated from a latent state $\widetilde{\boldsymbol{Z}}_i$. The frames generated in the entire time is referred to as $\widetilde{\boldsymbol{\mathcal{I}}}_{0:T}$ for easy notations. The latent state has ground truth information of the frame being reconstructed, and the model is encouraged to use it during training. This is a conditional

version of the variational autoencoder, where the encoder and decoder are conditioned on the previous frame. $\mathcal{L}_{recon}$ computes the pixel-level L_1 distance between the predicted video frame and the ground truth frame.

$$\mathcal{L}_{recon} = \mathbb{E}_{\widetilde{\mathcal{I}}_i \sim p(\widetilde{\boldsymbol{\mathcal{I}}}_{0:T})} \left\| \widetilde{\mathcal{I}}_i - \mathcal{I}_i \right\|_1 \tag{4}$$

4.5.2 Adversarial Loss

Without overcoming the problem of modeling pixel covariances, it is likely not possible to produce sharp and clean predictions. The variational autoencoder tends to produce blurry images [11]. We can force the predictions to stay on the manifold by matching the distributions of the predicted and real sequences. We adopt two discriminators, one at the image level and the other at the video sequence level, to improve the output quality both in spatial appearance and temporal dynamics. Given a discriminator D in Figure.2 that is capable of distinguishing generated frames $\widetilde{\boldsymbol{\mathcal{I}}}_T$ from ground truth $\boldsymbol{\mathcal{I}}_T$. Specifically, we consist GAN architecture [2] to model D as,

$$\begin{aligned} \min_{\mathcal{D}_{img}} \max \mathcal{L}_{adv}^{img} &= \mathbb{E}_{\widetilde{\mathcal{I}}_i \sim p(\widetilde{\boldsymbol{\mathcal{I}}}_{0:T})}[(\mathcal{D}(\widetilde{\mathcal{I}}_i) - 1)^2] \\ &+ \mathbb{E}_{\widetilde{\mathcal{I}}_i \sim p(\widetilde{\boldsymbol{\mathcal{I}}}_{0:T})}[(\mathcal{D}(\text{E2V-SDE}(\widetilde{\mathcal{I}}_i | \boldsymbol{E}_{0:T})))^2], \end{aligned} \tag{5}$$

where $\boldsymbol{E}_{0:T}$ mean grid-voxel type inputs in the entire time.

4.5.3 Temporal Consistency Loss

The network relies on the recurrent connection to naturally enforce temporal consistency between successive reconstructions. However, some temporal artifacts may remain, such as blinking, which is especially noticeable in homogeneous image regions. To address this issue, we introduce an explicit temporal consistency loss based on [19].

$$\mathcal{L}_{tc} = \mathbb{E}_{\widetilde{\mathcal{I}}_i \sim p(\widetilde{\boldsymbol{\mathcal{I}}}_{0:T})} \psi_{t,t-1} \left\| \widetilde{\mathcal{I}}_i - \mathcal{W}(\mathcal{F}_i, \widetilde{\mathcal{I}}_i) \right\|_1, \tag{6}$$

where $\psi_{t,t-1} = \exp(-\alpha \left\| \mathcal{I}_t - \mathcal{W}(\mathcal{F}_i, \widetilde{\mathcal{I}}_i) \right\|_2^2)$ is the visibility mask calculated from the warping error between the ground truth $\mathcal{I}_i$ and the warped input frame $\mathcal{W}(\mathcal{F}_i, \widetilde{\mathcal{I}}_i)$ and α is set to be 50.

4.5.4 Difference Loss

$\mathcal{L}_{diff}$ helps the model learn the image difference $\mathcal{D}_i$ as the pixel-wise difference between consecutive video frames.

$$\mathcal{L}_{diff} = \mathbb{E} \left\| \mathcal{D}_i - \Delta \mathcal{I}_{i-1:i} \right\|_1, \tag{7}$$

where $\Delta \mathcal{I}_{i-1:i}$ denotes the image difference between two adjacent frames, $i.e, \mathcal{I}_i - \mathcal{I}_{i-i}$.

4.6. Overall Objective

E2V-SDE is trained end-to-end using the following objective function as,

$$\mathcal{L} = \mathcal{L}_{recon} + \lambda_{adv}\mathcal{L}_{adv} + \lambda_{tc}\mathcal{L}_{tc} + \lambda_{diff}\mathcal{L}_{diff}. \tag{8}$$

5. Experiments and Results

5.1. Experimental Setup

Training dataset An ideal simulated dataset for high-speed HDR video reconstruction should meet several criteria, that is, high speed, HDR, and neither background nor foreground is static. Many previous works [34, 37, 44] used ESIM simulator [33] to render events from images along the virtual camera trajectory. This approach provides sufficient training data, which is beneficial for learning-based methods. To make a fair comparison, we follow the same generation scheme as E2VID [34] to synthesize the training dataset via ESIM. In addition to decide the contrast thresholds (CTs), we follow as same as the proposed method in [39].

Following the training setting used by [34], we adopt the same training data augmentation strategy. Gaussian noise of $\mathcal{N}(\mu = 0, \sigma = 0.1)$ is added to every temporal bin in each event tensor within a sequence. We perform random cropping with a size of 112×112 and further augment data using random horizontal, vertical and polarity flips, besides with artificial pauses of the input event stream.

Test dataset We evaluate our model on three publicly released event-based datasets: HQF [39], IJRR [27] and MVSEC [45]. HQF is presented in [39] for providing ground truth DAVIS frames that are minimally motion-blurred and well-posed. IJRR [27] are released in a collection of datasets captured with a DAVIS in a variety of synthesized and real environments. Scenes in MVSEC are recorded by a synchronized stereo event camera system. Each sequence of MVSEC provides extensive ground truth reference data for evaluations. Unlike HQF, IJRR and MVSEC are not designed specifically for the event-based video reconstruction task.

Evaluation metric We measure the scores obtained from three evaluation metrics for quantitative evaluation of E2V-SDE: mean squared error (MSE), structural similarity (SSIM) and perceptual similarity (LPIPS).

Implementation details Our network is implemented using the Pytorch framework. We employ Adam optimizer [17], a widely-used optimization method to iteratively train E2V-SDE. We train our model for 300 epochs with a batch size of 2 on a single NVIDIA TITAN RTX GPU. The learning rate is set initially as 0.001, then exponentially decayed at a rate of 0.99 per epoch. For hyperparameter of our model, we use $\lambda_{diff} = 1.0$, $\lambda_{adv} = 0.005$, $\lambda_{tc} = 0.005$, and

Table 1. Quantitative comparison of baseline methods of event-based video reconstruction on HQF, IJRR and MVSEC. The values in bold correspond to the best values in each metric. All models were executed without minmax normalization. E2V-ODE is a model without stochastic term (wiener process).

Method	MSE ↓			SSIM ↑			LPIPS ↓		
	HQF	IJRR	MVSEC	HQF	IJRR	MVSEC	HQF	IJRR	MVSEC
E2VID [34]	0.190	0.175	0.382	0.469	0.486	0.208	0.512	0.371	0.693
E2VID+ [39]	0.037	0.065	0.135	0.638	0.551	0.337	0.258	0.241	0.513
FireNet [37]	0.098	0.132	0.263	0.498	0.508	0.238	0.462	0.354	0.653
FireNet+ [39]	0.047	0.057	0.228	0.595	0.535	0.265	0.326	0.298	0.574
ET-Net [44]	**0.034**	0.051	0.087	0.646	0.600	0.361	0.282	0.263	0.482
E2V-ODE (ours)	0.042	0.097	0.121	0.618	0.588	0.288	0.276	0.258	0.447
E2V-SDE (ours)	0.041	**0.046**	**0.079**	**0.696**	**0.658**	**0.373**	**0.251**	**0.240**	**0.425**

$\lambda_{diff} = 0.025$. Detailed information about implementation is given in the appendix.

5.2. Results

We compare our proposed method with five existing methods: E2VID [34], E2VID+ [39], FireNet [37], FireNet+ [39] and ET-Net [44]. E2VID+ and FireNet+ are the improved versions of E2VID and FireNet, respectively, sharing their same architectures but retrained with the method as described in [39].

Image quality The quantitative results are listed in Table 1. Numbers of other methods are directly taken as mentioned in each paper and inferenced with published model without processing. Overall, E2V-SDE achieves state-of-the-art performance in all cases compared to baseline methods, except for only one case in which the value of MSE is slightly higher on HQF dataset. We think this is a a result of VAE architecture's inherent limitation known as blurry output [11]. In terms of SSIM, E2V-SDE constantly outperformed ET-Net, which had been by far the best performing method. Especially, there was a clear improvement when tested on HQF dataset, achieving a score of 0.696. LPIPS scores were also consistently low on all three datasets. As human can quickly evaluate the perceptual similarity between two images, LPIPS is a metric made to estimate that value. Therefore, our model's overwhelming LPIPS scores show that E2V-SDE can get the clearest and most well-reconstructed images for human perception.

Figure 3 presents the sample qualitative results reconstructed by E2V-SDE and all baseline methods on images of video clips from the HQF, IJRR and MVSEC datasets. The ground-truth images are also included for comparison. We did not adjust any post-processing like local histogram equalization. Overall, what stands out is that the results of our model are images with higher intensity in all circumstance, even when viewed with the naked eye compared to other models, and it is possible to distinguish objects with sharp edges. One of the most prominent features is the reconstructed frames of MVSEC dataset depicted in row 6 of Figure 3. Compared to the ground truth, the reconstructed image from our model is sharper and more recognizable. The scene is reconstructed based on a outdoor_day1 in MVSEC dataset recorded through DAVIS while actually driving outdoor. This shows the possibility that our model could be applied in real life. More resulting frames sampled from the three datasets are provided in the appendix.

Table 2. Averaged reconstruction time per image and the number of parameters of the models.

Method	Params.	Recon. time (ms/img) ↓		
	(M) ↓	HQF	IJRR	MVSEC
E2VID [34]	10.71	3.72	6.24	5.11
FireNet [37]	0.04	2.67	3.16	2.29
ET-Net [44]	16.63	20.78	22.96	28.75
E2V-SDE (ours)	4.83	3.03	4.30	3.56

Size and reconstruction time Considering scalability to various fields in the future, inference speed and number of parameters are important issues. We measured the time a model requires to output each sample and included the comparison results along with the size of each model in Table 2. Compared to E2VID, E2V-SDE uses half the number of parameters and the reconstruction speed is faster by up to 31% depending on the dataset. As FireNet was designed to lighten E2VID and achieve a very high throughput, the parameter size is small and reconstruction speed is slightly faster than E2V-SDE. However, as a trade-off, the quality of the image is much improved in E2V-SDE. ET-Net produces relatively high-quality images when compared to E2VID and FireNet, but the complex operations of the Transformer architecture significantly delays the reconstruction time. E2V-SDE achieves higher image quality than ET-Net while reducing the reconstruction speed by 81-87%.

Use of SDE To prove the efficacy of SDE in event-based video reconstruction, we also trained E2V-ODE, which combines ConvGRU with general ODE, under the same training conditions and compared the results. The MSE,

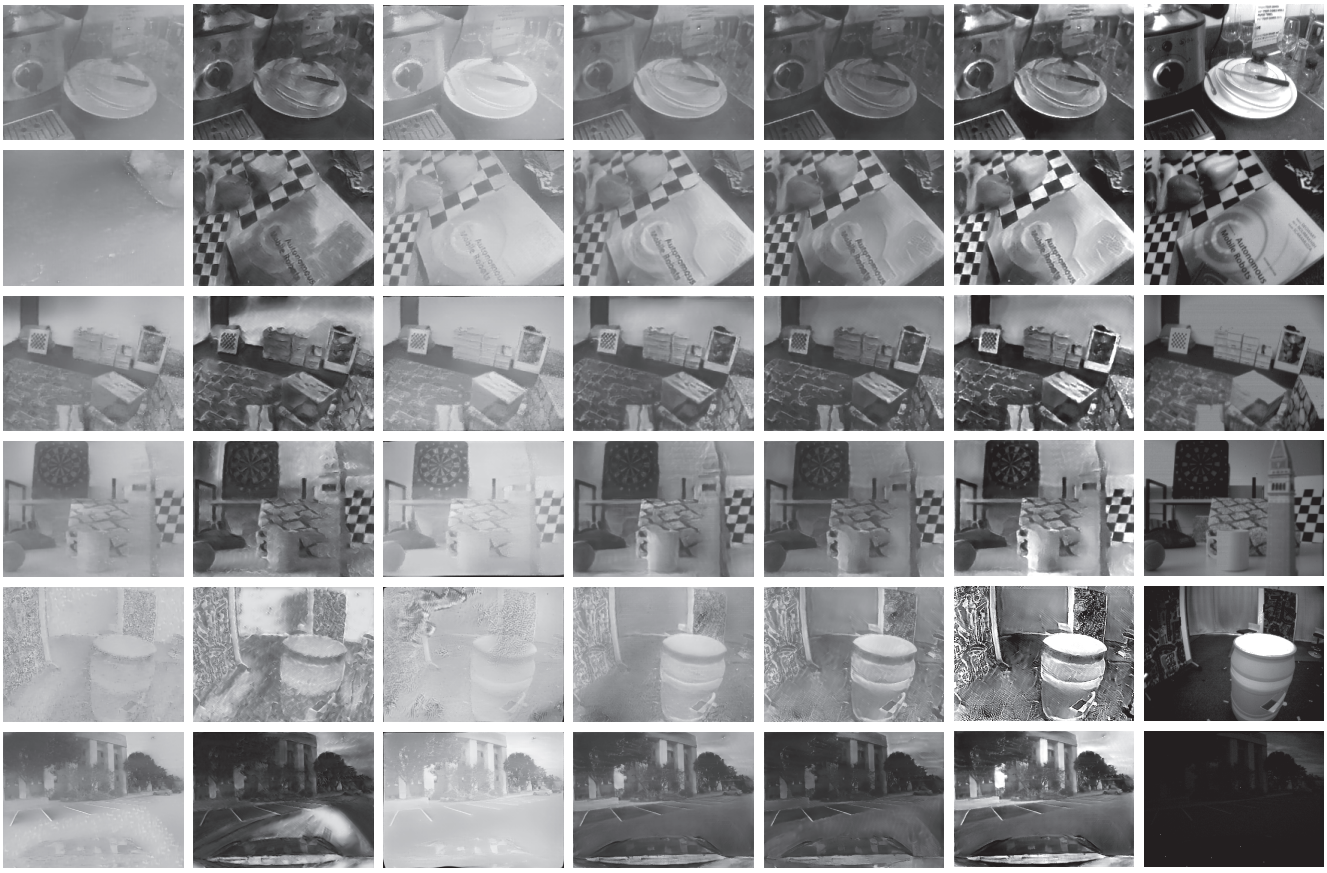

Figure 3. Qualitative comparison with baseline methods on HQF (Row 1&2), IJRR (Row 3&4) and MVSEC (Row 5&6). E2V-SDE demonstrates better reconstruction results with fine-grained details and minor artifacts, while other baselines present foggy effects, blurry images. More visual results can be found in the appendix.

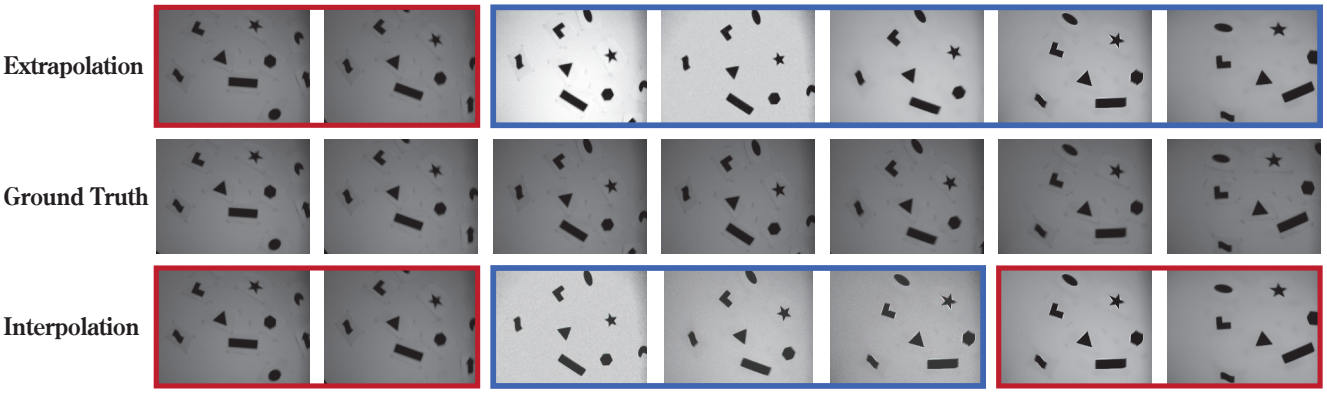

Figure 4. Qualitative results of extrapolation (top row) and interpolation (bottom row). The ground truth frames are placed in the middle row for comparison. Red boxes indicate observations, which are the given event streams for the extrapolation and interpolation.Blue boxes represent the predictions (generated frames) of E2V-SDE. Prior researches can not predict with given data if the models are fed empty event tensor. While Vid-ODE is successfully inferring video frames at unseen timesteps thanks to learning the underlying video dynamic. In this respect, E2V-SDE has significant scalability.

SSIM, and LPIPS values of E2V-ODE are also reported in Table 1. It can be seen from the results that E2V-ODE failed to fully learn the anomalous movements of the realistic scenes, giving inferior scores in all three datasets. We mentioned deterministic modeling for complex continuous-time stochastic processes as one of the reasons why video

Table 3. Ablation study for Components.Performance improvement by adding each component to the E2V-SDE suggesting the applicability of each component to improve performance of tasks.

Methods	MSE ↓			SSIM ↑			LPIPS ↓		
	HQF	IJRR	MVSEC	HQF	IJRR	MVSEC	HQF	IJRR	MVSEC
ODE-Conv	0.077	0.148	0.268	0.916	0.516	0.313	0.370	0.669	1.188
E2V-ODE	0.063	0.065	0.115	0.748	0.563	0.342	0.306	0.353	0.622
Vanilla E2V-SDE	0.071	0.093	0.163	0.842	0.534	0.324	0.341	0.397	0.701
+Adversarial learning	0.063	0.059	0.103	0.744	0.581	0.353	0.303	0.317	0.559
+Optical flow	0.058	0.049	0.087	0.689	0.593	0.360	0.282	0.267	0.471
+Flow valid mask	0.057	0.046	0.080	0.675	0.606	0.368	0.276	0.244	0.430
+Temporal consistency	**0.041**	**0.046**	**0.079**	**0.696**	**0.614**	**0.373**	**0.251**	**0.241**	**0.425**

reconstruction is difficult. Since ODE makes a deterministic assumption that the trajectory is determined when the initial value is determined, it can be seen that our model outperforms in a stochastic real-world situation.

5.3. Interpolation and Extrapolation

To handle the challenging scenes including motion blur, lighting change or occlusion inference, interpolation focuses on recovering intermediate frames between any two consecutive original video frames.

Extrapolation of a video is same as video synthesis which generates the succeeding video sequences based on few consecutive video frames. Apart from the superior video reconstruction ability of E2V-SDE as mentioned above, another advantage of E2V-SDE is that it can directly perform video interpolation and extrapolation tasks without additional training. Compared to previous works, our model incorporates the latent state trajectory to capture the underlying factors of the system dynamics.

As a result, E2V-SDE can also predict the future through currently observed events, which could not be done in previous studies. Sample interpolation and extrapolation results of E2V-SDE are presented in Figure 4. It can be seen that E2V-SDE seamlessly generates frame images of unobserved time domains in the middle or after the end by just looking at the given events. It can be seen that although it cannot predict an object suddenly appearing in the frame, it predicts that an object existing in the frame moves out of the frame.

5.4. Ablation Study

We investigated the effects of the components explained in Section 4.3 by conducting an ablation study. Table 3 depicts the effectiveness of each component of the E2V-SDE. Starting with a simple baseline ODE-Conv, we first compare E2V-ODE equipped with the proposed ODE-ConvGRU but didn't have randomness. We see a significant boost in performance, meaning that the ODE-ConvGRU cell better captures spatio-temporal dynamics in the video and is able to generate high-quality frames. Starting from vanilla E2V-SDE without any linear compositions, E2V-SDE yielded improved scores each time the remaining losses were added one by one (from 4th to 7th row). It can be seen that the performance difference between when the $\mathcal{L}_{adv}$ is applied and without $\mathcal{L}_{adv}$ is noticeable. In addition, it has been proven through the result of metric that adding the adversarial loss improves performance, especially in LPIPS, suggesting that the image and sequence discriminators help the model generate realistic images. The optical flow warping significantly enhances the performance by effectively learning the video dynamics. The performance boost from 6-th row to 7-th row might seem marginal.

6. Conclusion

In this work, we present E2V-SDE, a novel event-based video reconstruction model that uses a neural SDEs to learn the latent dynamics of event data in a continuous perspective and generates frames at any given timesteps In addition, we adopt a variational autoencoder, a discriminator and various image composition techniques, our model could generate high-quality images quickly and efficiently. Combining the SDE-ConvGRU with the linear composition of optical flow and image difference, our model successfully demonstrates its ability to generate high-quality video frames in the continuous-time domain. Compared to previous methods, the superiority of E2V-SDE is demonstrated through extensive experiments both qualitatively and quantitatively. In addition, the distinguishing feature of our model from other studies is that it is a model that can not only reconstruct video but also interpolate and extrapolate unseen data, which is expected to be applied to many studies in the future. Taking advantage of the capacity of neural SDEs, E2V-SDE has higher flexibility and generalizability in modeling the nonlinear stochastic dependency from high-dimensional observations.

Acknowledgements

This work was supported by Institute of Information & communications Technology Planning & Eval-

uation (IITP) grant funded by the Korea government(MSIT) [NO.2021-0-01343, Artificial Intelligence Graduate School Program (Seoul National University)], the National Research Foundation of Korea (NRF) grant funded by MSIT [NRF-2021M3F3A2A02037893] and [NRF-2021R1C1C2010454], the BK21 FOUR program of the Education and Research Program for Future ICT Pioneers, Seoul National University in 2022, and AIRS Company in Hyundai Moter Company & Kia Corporation through HMC/KIA-SNU AI Consortium Fund.

References

[1] Ellen Baake, Michael Baake, HG Bock, and KM Briggs. Fitting ordinary differential equations to chaotic data. *Physical Review A*, 45(8):5524, 1992. 2

[2] Andrew Brock, Jeff Donahue, and Karen Simonyan. Large scale gan training for high fidelity natural image synthesis. *arXiv preprint arXiv:1809.11096*, 2018. 5

[3] Ricky TQ Chen, Yulia Rubanova, Jesse Bettencourt, and David Duvenaud. Neural ordinary differential equations. *arXiv preprint arXiv:1806.07366*, 2018. 2

[4] Wei Chen, David Wipf, Yu Wang, Yang Liu, and Ian J Wassell. Simultaneous bayesian sparse approximation with structured sparse models. *IEEE Transactions on Signal Processing*, 64(23):6145–6159, 2016. 1

[5] Matthew Cook, Luca Gugelmann, Florian Jug, Christoph Krautz, and Angelika Steger. Interacting maps for fast visual interpretation. In *The 2011 International Joint Conference on Neural Networks*, pages 770–776. IEEE, 2011. 2

[6] Conor Durkan, Artur Bekasov, Iain Murray, and George Papamakarios. Neural spline flows. *Advances in Neural Information Processing Systems*, 32:7511–7522, 2019. 2

[7] Ronald M Errico. What is an adjoint model? *Bulletin of the American Meteorological Society*, 78(11):2577–2592, 1997. 2

[8] Guillermo Gallego, Tobi Delbruck, Garrick Orchard, Chiara Bartolozzi, Brian Taba, Andrea Censi, Stefan Leutenegger, Andrew Davison, Jörg Conradt, Kostas Daniilidis, et al. Event-based vision: A survey. *arXiv preprint arXiv:1904.08405*, 2019. 1

[9] Ali Hasan, João M Pereira, Sina Farsiu, and Vahid Tarokh. Identifying latent stochastic differential equations with variational auto-encoders. *arXiv preprint arXiv:2007.06075*, 2020. 3

[10] Liam Hodgkinson, Chris van der Heide, Fred Roosta, and Michael W Mahoney. Stochastic normalizing flows. *arXiv preprint arXiv:2002.09547*, 2020. 2

[11] Huaibo Huang, Zhihang Li, Ran He, Zhenan Sun, and Tieniu Tan. Introvae: Introspective variational autoencoders for photographic image synthesis. *arXiv preprint arXiv:1807.06358*, 2018. 5, 6

[12] Mike Innes, Alan Edelman, Keno Fischer, Chris Rackauckas, Elliot Saba, Viral B Shah, and Will Tebbutt. A differentiable programming system to bridge machine learning and scientific computing. *arXiv preprint arXiv:1907.07587*, 2019. 2

[13] Junteng Jia and Austin R Benson. Neural jump stochastic differential equations. *arXiv preprint arXiv:1905.10403*, 2019. 2

[14] Martin Jørgensen, Marc Deisenroth, and Hugh Salimbeni. Stochastic differential equations with variational wishart diffusions. In *International Conference on Machine Learning*, pages 4974–4983. PMLR, 2020. 2

[15] Patrick Kidger, James Foster, Xuechen Li, Harald Oberhauser, and Terry Lyons. Neural sdes as infinite-dimensional gans. *arXiv preprint arXiv:2102.03657*, 2021. 2, 3

[16] Hanme Kim, Ankur Handa, Ryad Benosman, Sio-Hoi Ieng, and Andrew J Davison. Simultaneous mosaicing and tracking with an event camera. *J. Solid State Circ*, 43:566–576, 2008. 2

[17] Diederik P Kingma and Jimmy Ba. Adam: A method for stochastic optimization. *arXiv preprint arXiv:1412.6980*, 2014. 5

[18] Lingkai Kong, Jimeng Sun, and Chao Zhang. Sde-net: Equipping deep neural networks with uncertainty estimates. *arXiv preprint arXiv:2008.10546*, 2020. 2

[19] Wei-Sheng Lai, Jia-Bin Huang, Oliver Wang, Eli Shechtman, Ersin Yumer, and Ming-Hsuan Yang. Learning blind video temporal consistency. In *Proceedings of the European conference on computer vision (ECCV)*, pages 170–185, 2018. 5

[20] Xuechen Li, Ting-Kam Leonard Wong, Ricky TQ Chen, and David Duvenaud. Scalable gradients for stochastic differential equations. In *International Conference on Artificial Intelligence and Statistics*, pages 3870–3882. PMLR, 2020. 2, 3

[21] Zachary C Lipton, David Kale, and Randall Wetzel. Directly modeling missing data in sequences with rnns: Improved classification of clinical time series. In *Machine learning for healthcare conference*, pages 253–270. PMLR, 2016. 2

[22] Xuanqing Liu, Si Si, Qin Cao, Sanjiv Kumar, and Cho-Jui Hsieh. Neural sde: Stabilizing neural ode networks with stochastic noise. *arXiv preprint arXiv:1906.02355*, 2019. 2

[23] Xuanqing Liu, Tesi Xiao, Si Si, Qin Cao, Sanjiv Kumar, and Cho-Jui Hsieh. How does noise help robustness? explanation and exploration under the neural sde framework. In *Proceedings of the IEEE/CVF Conference on Computer Vision and Pattern Recognition*, pages 282–290, 2020. 2

[24] Tim Loossens, Francis Tuerlinckx, and Stijn Verdonck. A comparison of continuous and discrete time modeling of affective processes in terms of predictive accuracy. *Scientific reports*, 11(1):1–11, 2021. 2

[25] Jakob H Macke, Lars Buesing, John P Cunningham, Byron M Yu, Krishna V Shenoy, and Maneesh Sahani. Empirical models of spiking in neural populations. In *Advances in Neural Information Processing Systems 24: 25th conference on Neural Information Processing Systems (NIPS 2011)*, pages 1350–1358, 2012. 2

[26] James Morrill, Cristopher Salvi, Patrick Kidger, and James Foster. Neural rough differential equations for long time series. In *International Conference on Machine Learning*, pages 7829–7838. PMLR, 2021. 2

[27] Elias Mueggler, Henri Rebecq, Guillermo Gallego, Tobi Delbruck, and Davide Scaramuzza. The event-camera dataset

and simulator: Event-based data for pose estimation, visual odometry, and slam. *The International Journal of Robotics Research*, 36(2):142–149, 2017. 5

[28] Anh Nguyen, Thanh-Toan Do, Darwin G Caldwell, and Nikos G Tsagarakis. Real-time 6dof pose relocalization for event cameras with stacked spatial lstm networks. In *Proceedings of the IEEE/CVF Conference on Computer Vision and Pattern Recognition Workshops*, pages 0–0, 2019. 1

[29] Viktor Oganesyan, Alexandra Volokhova, and Dmitry Vetrov. Stochasticity in neural odes: An empirical study. *arXiv preprint arXiv:2002.09779*, 2020. 2

[30] Bernt Øksendal. Stochastic differential equations. In *Stochastic differential equations*, pages 65–84. Springer, 2003. 2

[31] Bernt Oksendal. *Stochastic differential equations: an introduction with applications*. Springer Science & Business Media, 2013. 3

[32] Christopher Rackauckas, Yingbo Ma, Julius Martensen, Collin Warner, Kirill Zubov, Rohit Supekar, Dominic Skinner, Ali Ramadhan, and Alan Edelman. Universal differential equations for scientific machine learning. *arXiv preprint arXiv:2001.04385*, 2020. 2

[33] Henri Rebecq, Daniel Gehrig, and Davide Scaramuzza. Esim: an open event camera simulator. In *Conference on Robot Learning*, pages 969–982. PMLR, 2018. 5

[34] Henri Rebecq, René Ranftl, Vladlen Koltun, and Davide Scaramuzza. High speed and high dynamic range video with an event camera. *IEEE transactions on pattern analysis and machine intelligence*, 2019. 1, 2, 3, 5, 6

[35] Olaf Ronneberger, Philipp Fischer, and Thomas Brox. U-net: Convolutional networks for biomedical image segmentation. In *International Conference on Medical image computing and computer-assisted intervention*, pages 234–241. Springer, 2015. 2

[36] Tom Ryder, Andrew Golightly, A Stephen McGough, and Dennis Prangle. Black-box variational inference for stochastic differential equations. In *International Conference on Machine Learning*, pages 4423–4432. PMLR, 2018. 2

[37] Cedric Scheerlinck, Henri Rebecq, Daniel Gehrig, Nick Barnes, Robert Mahony, and Davide Scaramuzza. Fast image reconstruction with an event camera. In *Proceedings of the IEEE/CVF Winter Conference on Applications of Computer Vision*, pages 156–163, 2020. 1, 2, 5, 6

[38] Yang Song, Jascha Sohl-Dickstein, Diederik P Kingma, Abhishek Kumar, Stefano Ermon, and Ben Poole. Score-based generative modeling through stochastic differential equations. *arXiv preprint arXiv:2011.13456*, 2020. 2

[39] Timo Stoffregen, Cedric Scheerlinck, Davide Scaramuzza, Tom Drummond, Nick Barnes, Lindsay Kleeman, and Robert Mahony. Reducing the sim-to-real gap for event cameras. In *Computer Vision–ECCV 2020: 16th European Conference, Glasgow, UK, August 23–28, 2020, Proceedings, Part XXVII 16*, pages 534–549. Springer, 2020. 5, 6

[40] Yifan Sun, Linan Zhang, and Hayden Schaeffer. Neupde: Neural network based ordinary and partial differential equations for modeling time-dependent data. In *Mathematical and Scientific Machine Learning*, pages 352–372. PMLR, 2020. 2

[41] Belinda Tzen and Maxim Raginsky. Neural stochastic differential equations: Deep latent gaussian models in the diffusion limit. *arXiv preprint arXiv:1905.09883*, 2019. 2

[42] Ashish Vaswani, Noam Shazeer, Niki Parmar, Jakob Uszkoreit, Llion Jones, Aidan N Gomez, Łukasz Kaiser, and Illia Polosukhin. Attention is all you need. In *Advances in neural information processing systems*, pages 5998–6008, 2017. 2

[43] Lin Wang, Yo-Sung Ho, Kuk-Jin Yoon, et al. Event-based high dynamic range image and very high frame rate video generation using conditional generative adversarial networks. In *Proceedings of the IEEE/CVF Conference on Computer Vision and Pattern Recognition*, pages 10081–10090, 2019. 1, 2

[44] Wenming Weng, Yueyi Zhang, and Zhiwei Xiong. Event-based video reconstruction using transformer. In *Proceedings of the IEEE/CVF International Conference on Computer Vision*, pages 2563–2572, 2021. 1, 2, 3, 5, 6

[45] Alex Zihao Zhu, Dinesh Thakur, Tolga Özaslan, Bernd Pfrommer, Vijay Kumar, and Kostas Daniilidis. The multivehicle stereo event camera dataset: An event camera dataset for 3d perception. *IEEE Robotics and Automation Letters*, 3(3):2032–2039, 2018. 5

[46] Xueyan Zou, Linjie Yang, Ding Liu, and Yong Jae Lee. Progressive temporal feature alignment network for video inpainting. In *Proceedings of the IEEE/CVF Conference on Computer Vision and Pattern Recognition*, pages 16448–16457, 2021. 4